An Early-Branching Microbialite Cyanobacterium Forms Intracellular Carbonates

Estelle Couradeau,[1,2,3] Karim Benzerara,[1]* Emmanuelle Gérard,[2] David Moreira,[3] Sylvain Bernard,[4] Gordon E. Brown Jr.,[5,6] Purificación López-García[3]

Cyanobacteria have affected major geochemical cycles (carbon, nitrogen, and oxygen) on Earth for billions of years. In particular, they have played a major role in the formation of calcium carbonates (i.e., calcification), which has been considered to be an extracellular process. We identified a cyanobacterium in modern microbialites in Lake Alchichica (Mexico) that forms intracellular amorphous calcium-magnesium-strontium-barium carbonate inclusions about 270 nanometers in average diameter, revealing an unexplored pathway for calcification. Phylogenetic analyses place this cyanobacterium within the deeply divergent order Gloeobacterales. The chemical composition and structure of the intracellular precipitates suggest some level of cellular control on the biomineralization process. This discovery expands the diversity of organisms capable of forming amorphous calcium carbonates.

Cyanobacteria constitute a phylogenetically diverse group of bacteria that can carry out oxygenic photosynthesis (*1*). These cosmopolitan microorganisms occupy a wide array of terrestrial, marine, and freshwater habitats. They are major modern primary producers, as exemplified by the two marine cyanobacterial genera *Prochloroccocus* and *Synechoccocus*, which are responsible for 25% of global photosynthesis (*2*). In addition to their evolutionary importance as ancestors of chloroplasts in photosynthetic eukaryotes (*1*), cyanobacteria have an extensive fossil record. Calcified cyanobacteria commonly occur since the base of the Cambrian, the earliest undisputed occurrence being *Girvanella* at 700 million years ago (*3*). Moreover, the occurrence of massive fossil stromatolites likely traces their emergence back to at least 2.7 billion years ago (*4*). Since then, they have played a major role in the carbon cycle by converting CO_2 into organic carbon and carbonates (*2*) and incidentally enriching the atmosphere in oxygen (*5*).

Carbonate precipitation by some cyanobacteria results from their photosynthetic activity (*6*, *7*). Photosynthesis locally increases the concentration of CO_3^{2-} through the disproportionation of bicarbonate to carbonate and CO_2, which is fixed by ribulose-1,5-bisphosphate carboxylase-oxygenase (RuBisCO). The export of alkalinity from the intracellular to the extracellular medium involves a mechanism that is still poorly documented. This export process raises the saturation index of the surrounding microenvironment for carbonate minerals, leading to mineral precipitation if free cations (e.g., Ca^{2+}) and nucleation sites are available (*6*). In all cases described so far [e.g., (*2*, *8*)], carbonate mineral precipitation by cyanobacteria is extracellular. As a result, the chemical composition of precipitates depends essentially on the surrounding environmental conditions, with little control by the cell (*9*). Calcification efficiency varies among different species as a function of extracellular surface properties, including exopolymer composition (*10*) or varying physiological states of the cell (*11*, *12*). However, cyanobacterial calcification has been studied only in a few model species; thus, our knowledge of the mechanisms involved remains limited to a narrow phylogenetic window.

We studied biofilms dominated by cyanobacteria derived from modern microbialites collected in the highly alkaline (pH ~8.9) Lake Alchichica, Mexico (*13*). Previous studies have detected a large diversity of bacteria and microbial eukaryotes in these samples, plus a minor archaeal component (*14*, *15*). Alchichica microbialites are mostly composed of hydromagnesite [$Mg_5(CO_3)_4(OH)_2{\cdot}4(H_2O)$] and aragonite ($CaCO_3$). In the course of long-term studies of Alchichica microbialites maintained in laboratory aquaria, we observed the conspicuous development of phototrophic biofilms on aquarium walls (fig. S1). The biofilms were dominated by cyanobacteria of different sizes and morphotypes (*13*), also recognizable by confocal laser scanning microscopy (CLSM) according to their red autofluorescence (using a green excitation wavelength). Among these different morphotypes, one relatively small, rod-shaped, unicellular morphotype was particularly abundant (fig. S1). These cells measured 3.9 ± 0.6 μm in length and 1.1 ± 0.1 μm in width and exhibited a granular cytoplasm (Fig. 1, A and B, and table S1). Autofluorescence emission spectra measured on individual cells showed the presence of chlorophyll and phycocyanin, supporting their identification as cyanobacteria (fig. S2). Scanning electron microscopy (SEM) revealed spherical intracellular granules in this morphotype with average diameter of 270 ± 44 nm (Fig. 1, C to I, and table S1). The average number of inclusions per cell was 21 ± 5. These inclusions were very bright in backscattered electron and secondary electron modes, suggesting that they contained elements of high atomic number. Their chemical composition was determined by energy-dispersive x-ray spectroscopy (EDXS; Fig. 2A). Inclusions contained Ca, Mg, Ba, and Sr as major elements with atomic ratios Ca/Mg = 2.88, Ba/Mg = 1.11, and Sr/Mg = 0.42 (table S2). These ratios were markedly different from those measured in the solution; relative to the medium where cells grew, Ba/Ca and Sr/Ca atomic ratios in the inclusions were higher by factors of 1370 and 86, respectively (tables S2 and S3).

We investigated the chemical composition and structure of the Ca-Mg-Sr-Ba inclusions with the use of transmission electron microscopy (TEM) and scanning transmission x-ray microscopy (STXM) (*13*). STXM allows imaging and acquisition of x-ray absorption near-edge structure (XANES) spectra at high spectral (~0.1 eV) and spatial (~25 nm) resolution. A peak at 290.3 eV in the XANES spectra measured at the C K-edge on intracellular inclusions (Fig. 2C and table S4) was attributed unambiguously to 1s-π* electronic transitions in carbonate groups (*16*). Selected-area electron diffraction patterns obtained by TEM on these inclusions suggested that they are amorphous (Fig. 2B). XANES spectra at the Ca $L_{2,3}$ edges are indicative of the local structure around Ca and can be used to characterize poorly organized phases [e.g., (*16*, *17*)]. Spectra measured on intracellular inclusions were different from spectra of common reference Ca carbonates such as aragonite, calcite, or Ca-substituted strontianite, but they were very similar to the spectrum of benstonite, a Mg-Ca-Sr-Ba carbonate (Fig. 2D and table S5). The stoichiometric formula of the intracellular inclusions can thus be written as $(Sr_1Ba_{2.7}Mg_{1.4}Ca_{0.9})Ca_6Mg(CO_3)_{13}$, following that of benstonite and in agreement with EDXS analyses. Hence, these intracellular inclusions are composed of an unusual benstonite-like phase with no long-range order and an unusual stoichiometry. In total, inclusions occupied ~6% of the total cell volume, raising the total density of the cells by 12% (tables S6 and S7).

We enriched these cyanobacteria in culture by inoculating modified BG11 medium with cells smaller than 3 μm from disrupted biofilms. CLSM and SEM observations showed that six enrichment cultures (out of 96) contained this single cyanobacterial morphotype with intracellular inclusions—that is, with no additional cyanobacterial morphotype as detected by microscopy

[1]Institut de Minéralogie et de Physique de la Matière Condensée, CNRS UMR 7590, Université Pierre et Marie Curie, 75005 Paris, France. [2]Institut de Physique du Globe de Paris (IPGP), CNRS UMR 7154, Université Paris Diderot, 75005 Paris, France. [3]Unité d'Ecologie, Systématique et Evolution, CNRS UMR 8079, Université Paris-Sud, 91405 Orsay Cedex, France. [4]Laboratoire de Minéralogie et de Cosmochimie du Museum (LMCM-MNHN), CNRS UMR 7202, 57 rue Cuvier, 75231 Paris Cedex 5, France. [5]Surface and Aqueous Geochemistry Group, Department of Geological and Environmental Sciences, Stanford University, Stanford, CA 94305, USA. [6]Department of Photon Science and Stanford Synchrotron Radiation Lightsource, SLAC National Accelerator Laboratory, 2575 Sand Hill Road, Menlo Park, CA 94025, USA.

*To whom correspondence should be addressed. E-mail: karim.benzerara@impmc.upmc.fr

(fig. S3). This was further confirmed by amplification and sequencing of 16*S* ribosomal RNA (rRNA) genes using cyanobacterial-specific primers, which provided 100% identical sequences within and among the six enrichments (table S8). Phylogenetic analysis showed that this strain was a member of the basal cyanobacterial order Gloeobacterales (Fig. 3).

The sequences obtained from the enrichment cultures were almost identical (99.7% sequence identity) to AQ1_1_1C_35 (CyanoOTU02) (*13*), an environmental sequence abundantly retrieved from aquarium microbialites (up to 20% of cyanobacterial sequences) (*15*). This indicates that this lineage is an important cyanobacterial component of actively growing microbialites, being able to disperse and form neighboring biofilms on aquarium walls. Because it is phylogenetically very distant from *Gloeobacter*, the only genus described within Gloeobacterales, we propose the following status: order Gloeobacterales, *Candidatus* Gloeomargarita lithophora gen. et sp. nov. (*13*).

The amorphous intracellular bioprecipitates are structurally and chemically different from the well-crystallized phases forming in the extracellular solution (i.e., aragonite and hydromagnesite) (tables S2 and S3). Incorporation of Sr and Ba in carbonates has implications for Sr/Ca and Ba/Ca ratios in marine carbonates, which are frequently used as paleoenvironmental proxies (*18*). Such proxies rely on the assumption that these ratios are approximately the same (or slightly lower) in the solid phases as in the solution. In *Candidatus* G. lithophora intracellular inclusions, these ratios are much higher in the solid phase and are similar to what has been found in some algae (*19*). Such an enrichment in Sr and Ba might involve active import systems specific for Sr^{2+} and Ba^{2+} and/or export systems extruding specifically Ca^{2+} and maintaining low cytoplasmic Ca^{2+} levels (*20*). The amorphous structure of the inclusions is somewhat similar to relatively unstable amorphous calcium carbonates (ACCs) observed in biological, mostly eukaryotic systems (*21*). Consistent with what has often been observed in these ACC-containing systems (*21*), the presence of organic macromolecules may

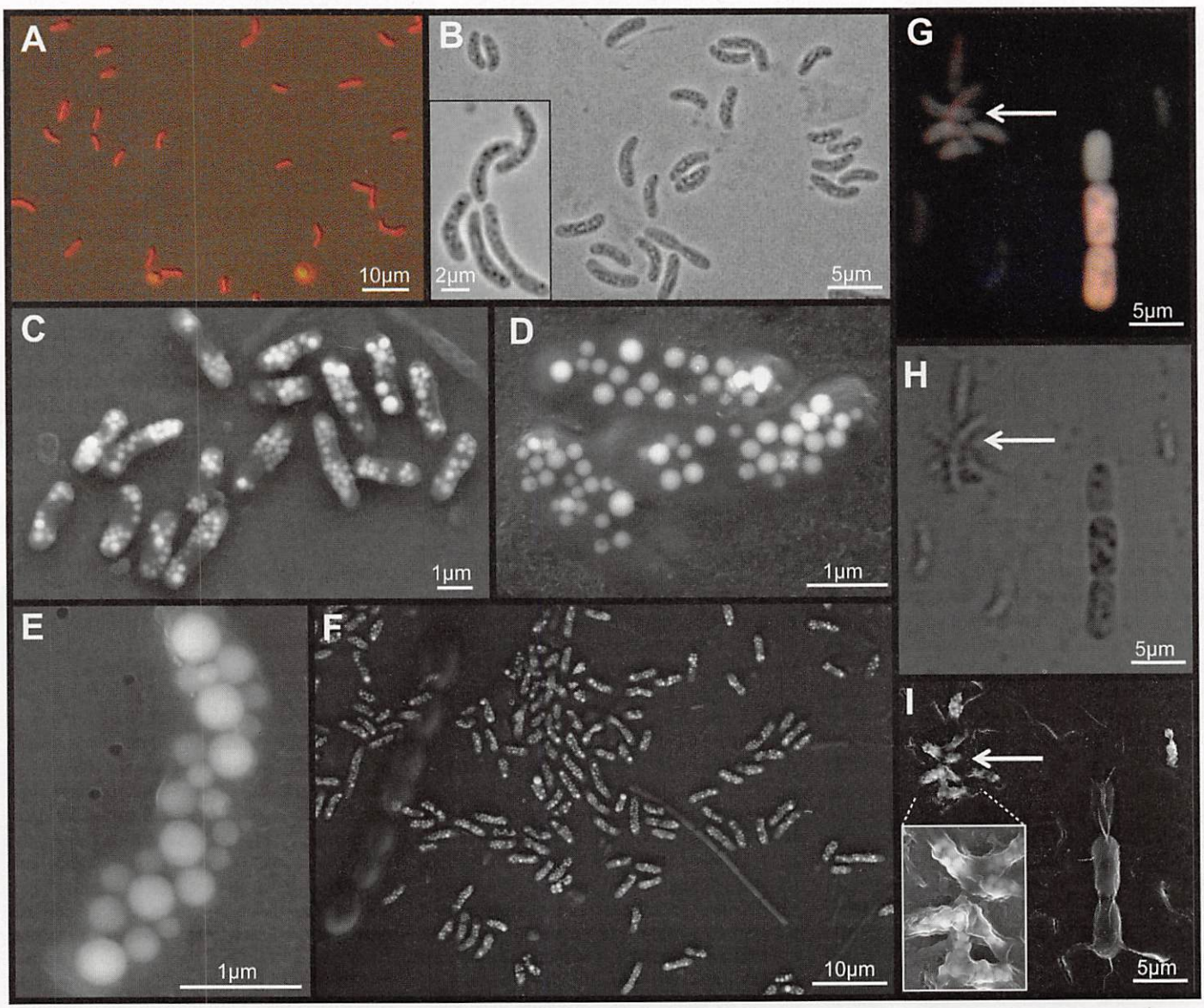

Fig. 1. Visualization of cyanobacterial cells forming intracellular mineral inclusions. (**A**) Composite epifluorescence and optical microscopy images showing rod-shaped autofluorescent cyanobacteria cells. (**B**) Optical image shows intracellular inclusions in cyanobacterial cells (higher magnification in inset). (**C** to **F**) SEM images (secondary electron mode) showing cells of the same morphotype, which systematically contain bright intracellular inclusions. (**G** to **I**) CSLM (G), phase contrast (H), and SEM (I) images of exactly the same area, showing that autofluorescent cells observed by CLSM contain the bright inclusions observed by SEM (inset). A different, larger, and inclusion-deprived cyanobacterial morphotype appears on the right.

stabilize the intracellular amorphous carbonates observed in *Candidatus* G. lithophora. Diverse local structures were recently suggested for these phases lacking long-range order (*22*). The Mg-, Ca-, Sr-, and Ba-containing inclusions expand the known diversity of ACC compositions.

Intracellular carbonate precipitation in this cyanobacterium likely influences its biology and ecology. First, by changing average cell density, these precipitates must alter cell buoyancy. The conspicuous occurrence of *Candidatus* G. lithophora in aquarium wall biofilms implies that a dispersive planktonic phase exists that allows the colonization of surrounding surfaces. Therefore, whereas gas vesicles function as flotation devices in planktonic cyanobacteria and other prokaryotes (*23*), intracellular carbonates might serve as ballast—an adaptation to a benthic mode of life. Second, the formation of intracellular carbonates implies that the alkalinity excess produced by cyanobacteria during photosynthetic carbon fixation, a process taking place in carboxysomes, is not always exported extracellularly but can be trapped within amorphous carbonate inclusions. Whether carboxysomes could also provide nucleation centers for carbonate precipitation remains an open question. Carbonate precipitation could act as a pH buffering system leading to an efficient carbon-concentrating mechanism and hence a high photosynthesis rate (*3*).

Because intracellular biomineralization occurs in a phylogenetically basal lineage of cyanobacteria that has retained ancestral characteristics (*24*) and because the alkalinity export may require the evolution of specific machinery, it might be argued that this calcification mode was performed by some ancestral cyanobacteria. Gloeobacterales is the only cyanobacterial order branching out before the chloroplast clade in molecular phylogenies of conserved gene markers (Fig. 3) (*25*). Not only *Gloeobacter violaceus*, isolated from limestone biofilms (*24*), but also most environmental sequences forming the large Gloeobacterales clade have been retrieved from rock-associated biofilms, stromatolites, or thermophilic microbial mats (Fig. 3). This association indicates a preference for these types of substrates and suggests that Gloeobacterales ancestors may have also exhibited the capacity to form biofilms in moderately hot and/or calcifying environments. Intracellularly biomineralizing cyanobacteria would not be prone to the formation of microfossils, in contrast to cyanobacteria inducing extracellular precipitation of carbonates within sheaths (*3*, *6*). As a result, microbialites dominated by intracellularly biomineralizing cyanobacteria might be devoid of microfossils. Alternatively, if they can be discriminated from abiotically formed phases (*26*), traces of this

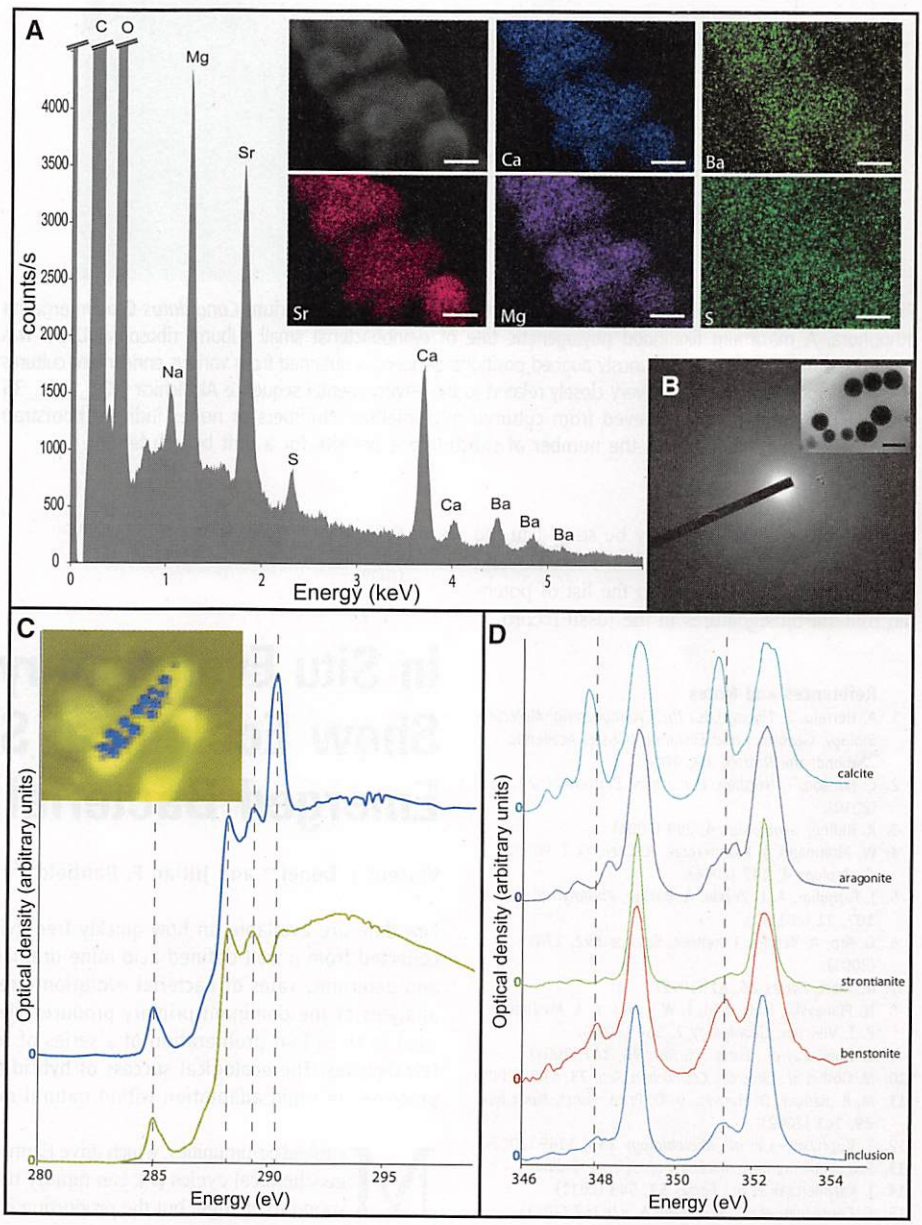

Fig. 2. Chemical and mineralogical characterization of intracellular inclusions. (**A**) SEM-EDXS spectrum and associated chemical maps obtained on inclusions (scale bars, 300 nm). Only Ca, Mg, Sr, and Ba are specifically associated with the inclusions, whereas S is distributed over the whole cells. (**B**) Selected-area electron diffraction pattern of an intracellular inclusion (inset; scale bar, 300 nm) showing a broad ring characteristic of an amorphous phase. (**C**) Average STXM-based XANES spectra with associated map (inset) measured at the C K-edge on areas showing only cellular material (yellow) and areas containing inclusions (blue). Spectra are shifted with respect to each other along the *y* axis for clarity; each spectrum has a different origin in *y*. Peak labels are reported in table S4. (**D**) STXM-based XANES spectrum measured at the Ca $L_{2,3}$-edges on intracellular inclusions. This spectrum is compared with spectra of reference calcite, aragonite, strontianite, and benstonite. The XANES spectrum of the intracellular inclusions matches that of benstonite in peak energy position and relative peak intensities. Peak positions are reported in table S5.

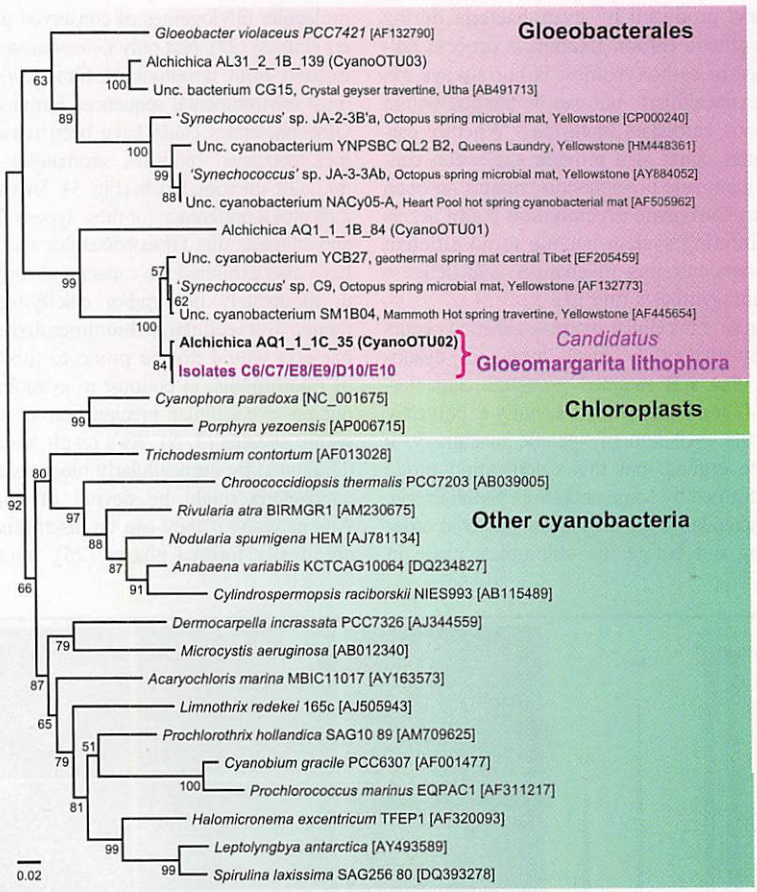

Fig. 3. Phylogenetic position of the intracellularly calcifying cyanobacterium *Candidatus* Gloeomargarita lithophora. A maximum likelihood phylogenetic tree of cyanobacterial small subunit ribosomal DNAs was constructed from 1191 unambiguously aligned positions. Sequences obtained from various enrichment cultures were 100% identical (pink) and very closely related to the environmental sequence Alchichica_AQ1_1_1C_35 CyanoOTU02, abundantly retrieved from cultured microbialites. Numbers at nodes indicate bootstrap values. The scale bar indicates the number of substitutions per site for a unit branch length.

biomineralization activity may be sought in the form of Ba- and Sr-rich carbonates. These Ba- and Sr-rich phases therefore add to the list of potential mineral biosignatures in the fossil record.

References and Notes

1. A. Herrero, E. Flores, Eds., *The Cyanobacteria: Molecular Biology, Genomics and Evolution* (Caister Academic, Wymondham, Norfolk, UK, 2008).
2. C. Jansson, T. Northen, *Curr. Opin. Biotechnol.* **21**, 365 (2010).
3. R. Riding, *Geobiology* **4**, 299 (2006).
4. W. Altermann, J. Kazmierczak, A. Oren, D. T. Wright, *Geobiology* **4**, 147 (2006).
5. J. Farquhar, A. L. Zerkle, A. Bekker, *Photosynth. Res.* **107**, 11 (2011).
6. G. Arp, A. Reimer, J. Reitner, *Science* **292**, 1701 (2001).
7. M. Merz, *Facies* **26**, 81 (1992).
8. N. Planavsky, R. P. Reid, T. W. Lyons, K. L. Myshrall, P. T. Visscher, *Geobiology* **7**, 566 (2009).
9. C. Dupraz *et al.*, *Earth Sci. Rev.* **96**, 141 (2009).
10. M. Obst *et al.*, *Geochim. Cosmochim. Acta* **73**, 4180 (2009).
11. M. R. Badger, D. Hanson, G. D. Price, *Funct. Plant Biol.* **29**, 161 (2002).
12. E. Kupriyanova *et al.*, *Microbiology* **153**, 1149 (2007).
13. See supplementary materials on *Science* Online.
14. J. Kaźmierczak *et al.*, *Facies* **57**, 543 (2011).
15. E. Couradeau *et al.*, *PLoS ONE* **6**, e28767 (2011).
16. K. Benzerara *et al.*, *Geobiology* **2**, 249 (2004).
17. M. E. Fleet, X. Y. Liu, *Am. Mineral.* **94**, 1235 (2009).
18. G. E. Bath *et al.*, *Geochim. Cosmochim. Acta* **64**, 1705 (2000).
19. M. R. Krejci *et al.*, *J. Struct. Biol.* **176**, 192 (2011).
20. D. C. Dominguez, *Mol. Microbiol.* **54**, 291 (2004).
21. L. Addadi, S. Raz, S. Weiner, *Adv. Mater.* **15**, 959 (2003).
22. P. Rez, A. Blackwell, *J. Phys. Chem. B* **115**, 11193 (2011).
23. A. E. Walsby, P. K. Hayes, R. Boje, *Eur. J. Phycol.* **30**, 87 (1995).
24. R. Rippka, J. Waterbury, G. Cohen-Bazire, *Arch. Microbiol.* **100**, 419 (1974).
25. L. I. Falcón, S. Magallón, A. Castillo, *ISME J.* **4**, 777 (2010).
26. E. Bittarello, D. Aquilano, *Eur. J. Mineral.* **19**, 345 (2007).

Acknowledgments: E.C. was recipient of a fellowship from the French Ministère de la Recherche et de l'Enseignement Supérieur. This project was financed by the CNRS interdisciplinary program "Environnements planétaires et origines de la vie" (PID EPOV) and Institut National des Sciences de l'Univers (INSU) program "InteractionsTerre/Vie" (InterrVie). The SEM facility of the Institut de Minéralogie et de Physique des Milieux Condensés is supported by Région Ile de France grant SESAME 2006 I-07-593/R, INSU-CNRS, INP-CNRS, University Pierre et Marie Curie, Paris. Support was also provided by NSF and the U.S. Environmental Protection Agency under cooperative agreement EF-0830093 through the Center for Environmental Implications of Nanotechnology. Advanced Light Source (ALS) Molecular Environmental Science beamline 11.0.2 is supported by the Office of Science, Office of Basic Energy Sciences, Division of Chemical Sciences, Geosciences, and Biosciences and Materials Sciences Division, U.S. Department of Energy, at the Lawrence Berkeley National Laboratory. Beamline 5.3.2 at ALS is supported by the Office of Basic Energy Sciences of the U.S. Department of Energy under contract DE-AC02-05CH11231. We thank R. Tavera (Universidad Autonónoma de México) for providing help as a field guide and the Laboratoire de Géochimie des Eaux at IPGP for providing the facility for Gran measurements. The sequence of the 16S rRNA gene of *Candidatus* Gloeomargarita lithophora has been deposited in GenBank under accession no. JQ733894. Data and enrichment cultures are available upon request.

Supplementary Materials

www.sciencemag.org/cgi/content/full/336/6080/459/DC1
Materials and Methods
Supplementary Text
Figs. S1 to S4
Tables S1 to S8
References (*27–38*)

3 November 2011; accepted 14 March 2012
10.1126/science.1216171

In Situ Evolutionary Rate Measurements Show Ecological Success of Recently Emerged Bacterial Hybrids

Vincent J. Denef[1]* and Jillian F. Banfield[1,2]†

Few data are available on how quickly free-living microorganisms evolve. We analyzed biofilms collected from a well-defined acid mine drainage system over 9 years to investigate the processes and determine rates of bacterial evolution directly in the environment. Population metagenomic analyses of the dominant primary producer yielded the nucleotide substitution rate, which we used to show that proliferation of a series of recombinant bacterial strains occurred over the past few decades. The ecological success of hybrid bacterial types highlights the role of evolutionary processes in rapid adaptation within natural microbial communities.

Microbial communities, which drive Earth's geochemical cycles (*1*), can rapidly respond to change, but the proportion of this response that can be attributed to evolutionary processes, rather than species composition or gene expression shifts, remains an unresolved